



Cite this: DOI: 10.1039/d2ee03358e

Spontaneous gas–solid reaction on sulfide electrolytes for high-performance all-solid-state batteries†

Xiao Zhang,^{ab} Xiaoyun Li,^{ab} Suting Weng,^{ac} Siyuan Wu,^{ac} Qiuyan Liu,^{ab} Mengyan Cao,^{ab} Yejing Li,^a Zhenyu Wang,^d Lingyun Zhu,^d Ruijuan Xiao,^{ib ac} Dong Su,^{ib ab} Xiqian Yu,^{ib ab} Hong Li,^{ib ac} Liqian Chen,^a Zhaoxiang Wang^{ib *ac} and Xuefeng Wang^{ib *abe}

Sulfide electrolytes with high ionic conductivity and facile formability are expected to replace the conventional flammable liquid electrolyte to construct high-energy and safe all-solid-state batteries (ASSBs). However, the practical use of sulfide electrolytes is mainly obstructed by their high sensitivity to humidity and instability to the high-voltage oxide cathodes. Herein, we solve these two problems of sulfide electrolytes by constructing a Li_2CO_3 interface through a spontaneous gas–solid reaction and achieve the enhanced electrochemical performance of ASSBs. Coupled with bare LiCoO_2 , the ASSBs with CO_2 -treated electrolyte or fabricated in a CO_2 -rich environment show impressive electrochemical performance with a remarkable rate performance (65 mA h g^{-1} at 3C) and excellent cycling retention (89.4% retention over 2100 cycles) at voltage up to 4.5 V vs. Li^+/Li . The improved performance is attributed to the enhanced interfacial stability with low resistance and demonstrates the practical feasibility and even superiority of sulfide electrolytes based on current battery fabrication conditions.

Received 17th October 2022,
Accepted 16th January 2023

DOI: 10.1039/d2ee03358e

rsc.li/ees

Broader context

All-solid-state batteries (ASSBs) are promising for next-generation battery technology due to their unique merits of integrated high energy density and high safety. The solid electrolyte used in the ASSBs should meet the requirements, such as (1) high ionic conductivity, (2) wide working voltage window, (3) easy fabrication, (4) high chemical stability, (5) low interfacial resistance, and (6) low cost. Among the various kinds of solid electrolytes, sulfide-based solid electrolytes outperform in their high ionic conductivity but need to improve their chemical/electrochemical compatibility with the moisture and high-voltage oxide-based cathode materials. In this work, we report a facile and universal gas–solid reaction to enhance the surface/interfacial stability of the sulfide electrolytes. Compared with conventional coating on the cathode particle, coating the sulfide electrolyte with Li_2CO_3 not only significantly reduces the interfacial reaction, but also enhances the air stability, which enables fabricating the sulfide electrolyte-based ASSBs in the dry room. Our findings provide a paradigm shift in sulfide electrolyte design and will accelerate the scalable application of sulfide-based ASSBs.

1. Introduction

As a next-generation energy storage power source, all-solid-state batteries (ASSBs) coupling Li metal anode with non-flammable solid electrolytes (SEs) are promising to solve the dilemma of high energy and high safety.^{1,2} Among various solid electrolyte candidates, sulfide solid electrolytes (SSEs) have attracted great attention owing to their high ionic conductivity (10^{-3} – $10^{-2} \text{ S cm}^{-1}$) and favorable formability.^{3–5} However, they are usually sensitive to humidity,^{6–8} which is a big challenge for fabrication and use. For example, the ionic conductivity of $\text{Li}_6\text{PS}_5\text{Cl}$ drops four orders of magnitude after exposure to humid air for 24 h.⁹ Partial substitution of S with O to form oxysulfide or substituting hard acid P^{5+} with soft

^a Beijing National Laboratory for Condensed Matter Physics, Institute of Physics, Chinese Academy of Sciences, Beijing 100190, China. E-mail: wxf@iphy.ac.cn, zxwang@iphy.ac.cn

^b College of Materials Science and Opto-Electronic Technology, University of Chinese Academy of Sciences, Beijing 100049, China

^c School of Physical Sciences, University of Chinese Academy of Sciences, Beijing 100049, China

^d Guilin Electrical Equipment Scientific Research Institute Co. Ltd., Guilin 541004, Guangxi, China

^e Tianmu Lake Institute of Advanced Energy Storage Technologies Co. Ltd., Liyang, 213300, Jiangsu, China

† Electronic supplementary information (ESI) available. See DOI: <https://doi.org/10.1039/d2ee03358e>

acids like As^{5+} or Sn^{4+} can alleviate the moisture sensitivity of SSEs.^{6,10–12}

Additionally, SSEs suffer from severe degradation when paired with high-voltage cathodes due to their intrinsic discrepancy in chemical potential, resulting in large interfacial resistance and inferior electrochemical performance of ASSBs to their liquid counterparts.^{11–14} To enable these high-voltage cathodes, such as LiCoO_2 , $\text{LiNi}_{0.8}\text{Co}_{0.15}\text{Al}_{0.05}\text{O}_2$, lithium-rich layered oxides for high-energy-density batteries, coating the cathode particles with some electronically insulated materials have become a routine method to reduce the interfacial reaction between SSEs and cathode materials, such as LiNbO_3 , $\text{Li}_4\text{Ti}_5\text{O}_{12}$, Li_3InCl_6 , *etc.*^{15–19} This strategy usually requires additional complex fabrication processes and it is hard to obtain a uniform coating layer. The insulating coating layer also obstructs the charge transfer between cathode particles resulting in sluggish kinetics.²⁰ Therefore, for more practical use, it is urgent to develop a new and facile solution to alleviate/solve the moisture sensitivity and interfacial stability of SSEs, which allows fabricating high-performance SSEs-based ASSBs based on the current battery manufacturing methods with minimal modification.

Herein, instead of coating the cathode materials, we provide a simple strategy to protect the SSEs by surface engineering through a gas–solid reaction, which could kill two birds with one stone. $\text{Li}_6\text{PS}_5\text{Cl}$ (LPSC) was used as a representative SSE and it reacts with some air components, such as O_2 and CO_2 spontaneously at room temperature. This reaction is facile and modifies the LPSC surface uniformly by either O-doping or amorphous Li_2CO_3 layer coating. Treatments in O_2 and CO_2 enhance the moisture toleration and interfacial stability of LPSC against bare LiCoO_2 effectively. In particular, the ASSBs with CO_2 -treated LPSC and bare LiCoO_2 exhibit a remarkable rate performance (65 mA h g^{-1} at 3C) and excellent cycling retention (89.4% retention over 2100 cycles) while operating at a voltage of up to 4.5 V *vs.* Li^+/Li . Using this strategy, we propose to fabricate the SSE-based ASSBs in a CO_2 -rich environment or a dry room and obtain superior electrochemical performance to that assembled in the Ar-filled glovebox. These demonstrations show the great potential of large-scale manufacturing of SSE-based ASSBs based on current battery manufacturing methods.

2. Results and discussion

2.1. Surface modification of $\text{Li}_6\text{PS}_5\text{Cl}$ electrolyte with flowing O_2/CO_2 gases

$\text{Li}_6\text{PS}_5\text{Cl}$ (LPSC) powder with a size range of 7–24 μm (Fig. S1a, ESI[†]) was treated in flowing pure O_2 or CO_2 gas at room temperature for different times (Fig. 1a and Fig. S2, ESI[†]). After the reaction, all the gas-treated LPSC samples maintain the pristine bulk structure without any new peak detected by X-ray diffraction (XRD, Fig. 1b). An increasing signal of CO_3^{2-} was found in CO_2 -treated LPSC *via* X-ray photoelectron spectroscopy (XPS, Fig. 1c) and Fourier transform infrared spectroscopy (FTIR, Fig. S3, ESI[†]) with increased exposure time,

indicating the spontaneous formation of the Li_2CO_3 layer on the surface of LPSC. The existence of the Li_2CO_3 shell was further confirmed by time-of-flight secondary-ion mass spectrometry (TOF-SIMS, Fig. S4, ESI[†]), and cryogenic TEM (Fig. 1d): LiC^- fragments were detected within ~ 400 s-sputtering depth (Fig. S4, ESI[†]); the electron energy loss spectroscopy (EELS) signal of Li_2CO_3 ^{21–23} was enriched at the surface (Fig. 1d) of the CO_2 -1h LPSC (stands for LPSC treated in CO_2 for 1 h). The resultant Li_2CO_3 is amorphous since none of its crystalline features are present in the XRD (Fig. S5, ESI[†]), selected area electron diffraction (Fig. S6a, ESI[†]), and high-resolution cryo-TEM image (Fig. S6b, ESI[†]). The thickness of the Li_2CO_3 layer was determined based on the EELS line scan results from typically three particles, which are 19–40 nm, 42–50 nm, 49–70 nm for CO_2 -0.5h, 1h, and 1.5h LPSC, respectively (Fig. 1e and Fig. S7, ESI[†]). Extending the reaction time or reducing the particle size of LPSC (*e.g.*, through ball milling, the size range of 400 nm–6 μm in Fig. S1b, ESI[†]) can exaggerate the reaction and yield a thicker Li_2CO_3 layer (Fig. 1e and Fig. S8, ESI[†]).

In terms of O_2 -treated LPSC, a new Raman peak (418 cm^{-1}) appears at the shoulder of the PS_4 vibration peak (425 cm^{-1} , Fig. S9, ESI[†]) after prolonged reaction, implying the formation of oxysulfide and is consistent with the previous reports.^{9,24–27} Long-time exposure in O_2 will over-oxidize the LPSC forming impurities and thus lead to a dramatical drop in ionic conductivity (Fig. S10, ESI[†]).

The reaction mechanism between LPSC and CO_2 was revealed by monitoring the releasing gases and weight change of LPSC *via in situ* thermogravimetric analysis coupled with mass spectrometry (TG-MS). As shown in Fig. 1f, CO gas was released steadily during CO_2 purging indicating that CO_2 reaction with LPSC results in Li_2CO_3 , lithium-deficient $\text{Li}_5\text{PS}_5\text{Cl}$, and CO:



This reaction is predicted to be thermodynamically feasible since its activation energy was estimated to be $-142.33 \text{ kJ mol}^{-1}$ (Fig. S11 and Table S1, ESI[†]) by density functional theory (DFT) calculations.

2.2. Electrochemical performance of the O_2/CO_2 -treated $\text{Li}_6\text{PS}_5\text{Cl}$ electrolyte

Pristine LPSC has a high ionic conductivity of 3 mS cm^{-1} (Fig. 2a). Gas treatment slightly lowers the ionic conductivity while O_2 -treated LPSCs show a slightly higher conductivity than the CO_2 -treated ones at the same exposure time. Among them, the CO_2 -1.5h LPSC exhibits the lowest conductivity of 0.3 mS cm^{-1} , which is close to that of the $\text{Li}_7\text{La}_3\text{Zr}_2\text{O}_{12}$ ^{28–30} and still acceptable for practical use. However, at the expense of ionic conductivity, gas treatment greatly enhances the moisture tolerance of LPSC, especially for CO_2 treatment. After storage in ambient air with a relative humidity of 17% for 1 h, pristine LPSC shows a dramatic conductivity drop by two magnitudes while the CO_2 -1h and CO_2 -1.5h treated samples maintain 54.0% and 80.9% of their conductivity (Fig. 2a). This demonstrates that

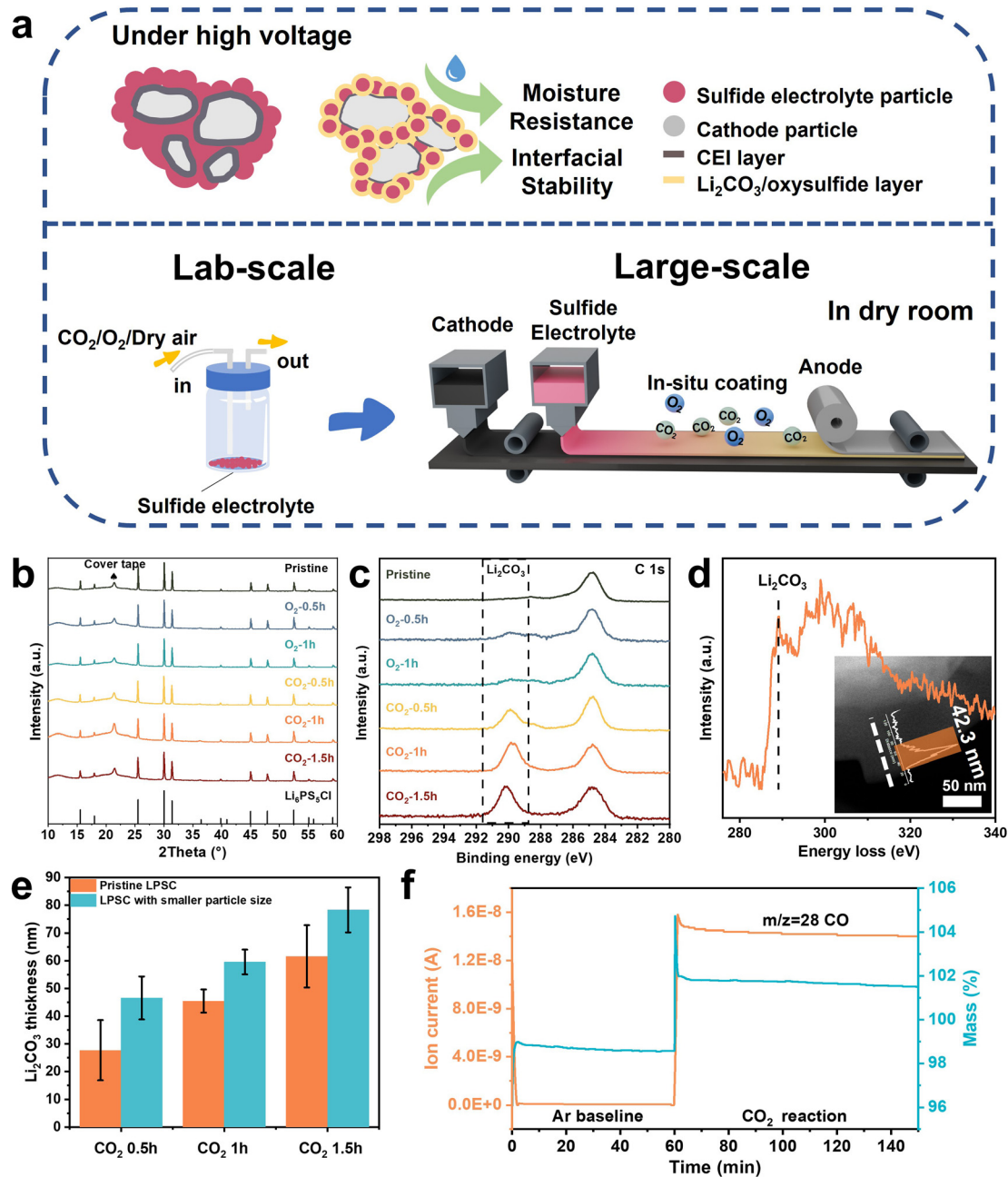


Fig. 1 The interaction between LPSC and O_2/CO_2 gases. (a) Schematic illustration of the solid–gas reaction and its application. (b) XRD spectra of the gas-treated LPSC samples. (c) XPS C 1s spectra of the CO_2 -treated LPSC. (d) EELS spectra of the C K-edge and the signal of C across the line scan acquired from the CO_2 -1h LPSC particle surface. (e) Li_2CO_3 thickness for the CO_2 -treated LPSC samples obtained from EELS line scan results. (f) Real-time gas evolution and weight change of the LPSC during CO_2 purging. The sudden increase in mass at immediate CO_2 purging (60 min) was attributed to buoyancy effects and the weight change of LPSC during the reaction was within the magnitude of instrumentation error.

the surface modification especially Li_2CO_3 coating can work as a shield protecting LPSC from external attacks, such as moisture and high-voltage cathode materials.

The electrochemical performances of ASSBs were evaluated with commercial bare $LiCoO_2$ (uncoated, clean surface, Fig. S12, ESI[†]) cycled between 4.5 V and 2.6 V versus Li^+/Li at room temperature. $LiCoO_2$ would react with pristine LPSC readily, resulting in an ASSB with a low initial coulombic efficiency (CE, 80.6%) and reversible capacity ($135.5 \text{ mA h g}^{-1}$)

(Fig. 2b), consistent with other reports.^{16,31,32} In contrast, post-treatment of LPSC with O_2/CO_2 indeed helps alleviate the side reactions leading to lower polarization, higher capacity of up to 160 mA h g^{-1} , and higher CE of over 85% (Fig. 2b). The rate capability was assessed over the current density ranging from 0.1C to 3C (Fig. 2c). It is obvious that all the ASSBs with O_2/CO_2 -treated LPSC display better rate capability than the pristine ones. Notably, the CO_2 -1h ASSB exhibited an impressive capacity of $\sim 65 \text{ mA h g}^{-1}$ at a rate of 3C. This indicates that the bulk ionic

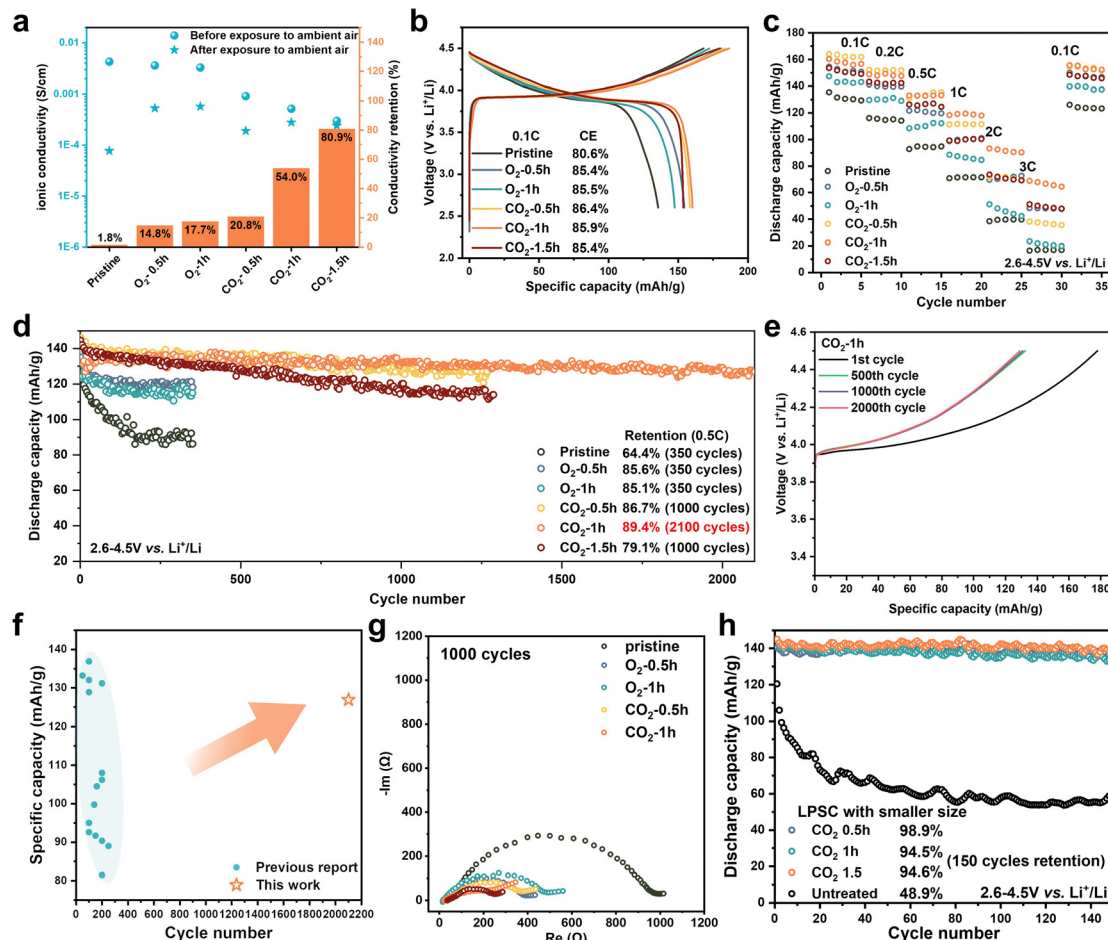


Fig. 2 Air stability of gas-treated LPSC and electrochemical performance of ASSBs with gas-treated LPSC as the electrolyte and bare LiCoO₂ as the cathode. (a) The ionic conductivity of gas-treated LPSC samples before and after exposure to ambient air with a relative humidity of 17% for 1 hour and its conductivity retention. (b) The initial charge–discharge voltage profiles between 2.6 and 4.5 V vs. Li⁺/Li at a 0.1C rate. (c) Rate performance ranging from 0.1C to 3C. (d) Long-term cycling performance at 0.5C. (e) The voltage profiles of ASSB with CO₂-1h LPSC during charging at different cycles. (f) Comparison of the electrochemical performance of LiCoO₂-based ASSBs with the literature. (Relevant references are listed in Table S2, ESI[†].) (g) Battery impedance after 1000 cycles. (h) Cycling performance at a 0.5C rate for LPSC after ball milling.

conductivity of SSEs is not the rate-determining step for the reaction kinetic of ASSBs, but interfacial stability is. In addition, the ASSBs with O₂/CO₂-treated LPSC also exhibit much more stable cycling and slower capacity fading compared with the pristine LPSC (Fig. 2d and Fig. S13, S14, ESI[†]). The ASSBs with CO₂-1h treated LPSC maintain 89.4% capacity at 0.5C over 2100 cycles and slight increase of polarization was observed from the 500th cycle to the 2000th cycle (Fig. 2e), which is better than most of the state-of-the-art LiCoO₂-based ASSBs (Fig. 2f). After 1000 cycles, it has a remarkably small interfacial resistance (278.4 Ω for the CO₂-1h sample vs. 959.6 Ω for the pristine one) suggesting the effective protection of the Li₂CO₃ shell as a buffer layer (Fig. 2g). This positive effect becomes pronounced when LPSC with a smaller particle size was used (Fig. 2h), which upon side reaction with cathode particles would be exaggerated (larger polarization and resistance in Fig. S15, ESI[†]) due to the enhanced particle contact, but significantly hindered by Li₂CO₃ coating. A combination result suggests a preferred thickness of the Li₂CO₃ layer of around 40–55 nm

(Fig. 1e, 2d and h), which is independent of the LPSC particle size and thick enough to eliminate the interfacial reaction between LPSC and LiCoO₂ with minimal sacrifice of LPSC ionic conductivity. Otherwise, the too low ionic conductivity of LPSC (such as 0.1 mS cm⁻¹ when LPSC was ball milled in a CO₂ atmosphere for 12 h) will increase the cell polarization and lead to a low reversible capacity (Fig. S16, ESI[†]).

This modification also works for other sulfide electrolytes, Li₇P₃S₁₁ for instance (Fig. S17, ESI[†]), or coupled with other high-voltage cathode materials such as LiNi_{0.815}Co_{0.15}Al_{0.035}O₂ (NCA) as well as Si/LCO full battery (Fig. S18, ESI[†]), showing much improved electrochemical performance. In addition, instead of totally replacing the pristine LPSC in both cathode composite and electrolyte, solely applying the CO₂-treated LPSC powder in the cathode composites (Fig. S19, ESI[†]) or using CO₂-treated LPSC pellets (Fig. S20, ESI[†]) as the electrolyte also work and show enhanced cycling stability compared to the pristine one. These performances are slightly worse than that totally using CO₂-treated LPSC, indicating that sufficient

interfacial protection is necessary to minimize the interfacial reactions on both cathode and anode sides.

2.3. Origin of superb cycling performance

The underlying origin of the superb cycling performance of CO₂-treated LPSC lies in its enhanced electrochemical stability. To figure out the nature of the cathode electrolyte interface (CEI), we first performed XPS on the cathode after 100 cycles. As seen in the S 2p spectra (Fig. 3a), apart from the main doublet associated with PS₄³⁻ (161.5 eV for S 2p_{3/2}),^{33,34} decomposition products including P₂S_x (163.4 eV),¹⁴ S (164.3 eV),^{35,36} Li₂S (160.0 eV),^{37,38} and SO₃²⁻ (167.1 eV)^{35,39} were detected on the LPSC surface. The continuous interfacial reaction significantly increases the resistance of the ASSBs compared with the pristine LPSC (Fig. 2f) while post-treating the LPSC with CO₂ largely enhances its interfacial stability and inhibits the side reactions as revealed by the weaker signals of these byproducts, especially for the CO₂-1h sample. This was further evidenced by the uniform distribution of P, and S elements around cathode particles (Fig. 3c and Fig. S21a, ESI[†]). However, for the pristine LPSC sample, P-rich regions can be observed (Fig. 3d and

Fig. S21b, ESI[†]), implying the formation of byproducts such as Li₃PO₄ or Li₃P.⁴⁰

To directly visualize the CEI, the 100-cycled cathode composites were scratched off for cryo-TEM characterization. A thick amorphous byproduct layer of ~22.7 nm with dispersed Li₂S nanograins was observed on the surface of LiCoO₂ coupled with the pristine LPSC (Fig. 4a). In contrast, only a ~4.2 nm CEI layer was formed on the surface of the LiCoO₂ particle with the CO₂-1h LPSC (Fig. 4b). EELS line scan results reveal the diffusion of Co and O elements (marked as the yellow shaded area in Fig. 4c, d and Fig. S22, ESI[†]), which show gradient distribution across the interface of the LiCoO₂/LPSC.⁴¹⁻⁴³ The thickness of the CEI layer measured by the EELS line scanning is roughly consistent with the HR-TEM observation. The thickness of Li₂CO₃ layer is reduced from original 42.3 nm (Fig. 1d) to 20.8 nm (marked as the blue-shaded area in Fig. 4d) after cycling suggesting the slight decomposition of Li₂CO₃ releasing CO₂ as detected by gas chromatography (Fig. S23, ESI[†]). Nevertheless, it is still working as a buffer layer between LPSC and LiCoO₂ and guaranteeing a long-term interfacial stability (Fig. 2d) due to its nonreactive nature to the LiCoO₂ (Fig. S24, ESI[†]) and potential self-limited kinetics.

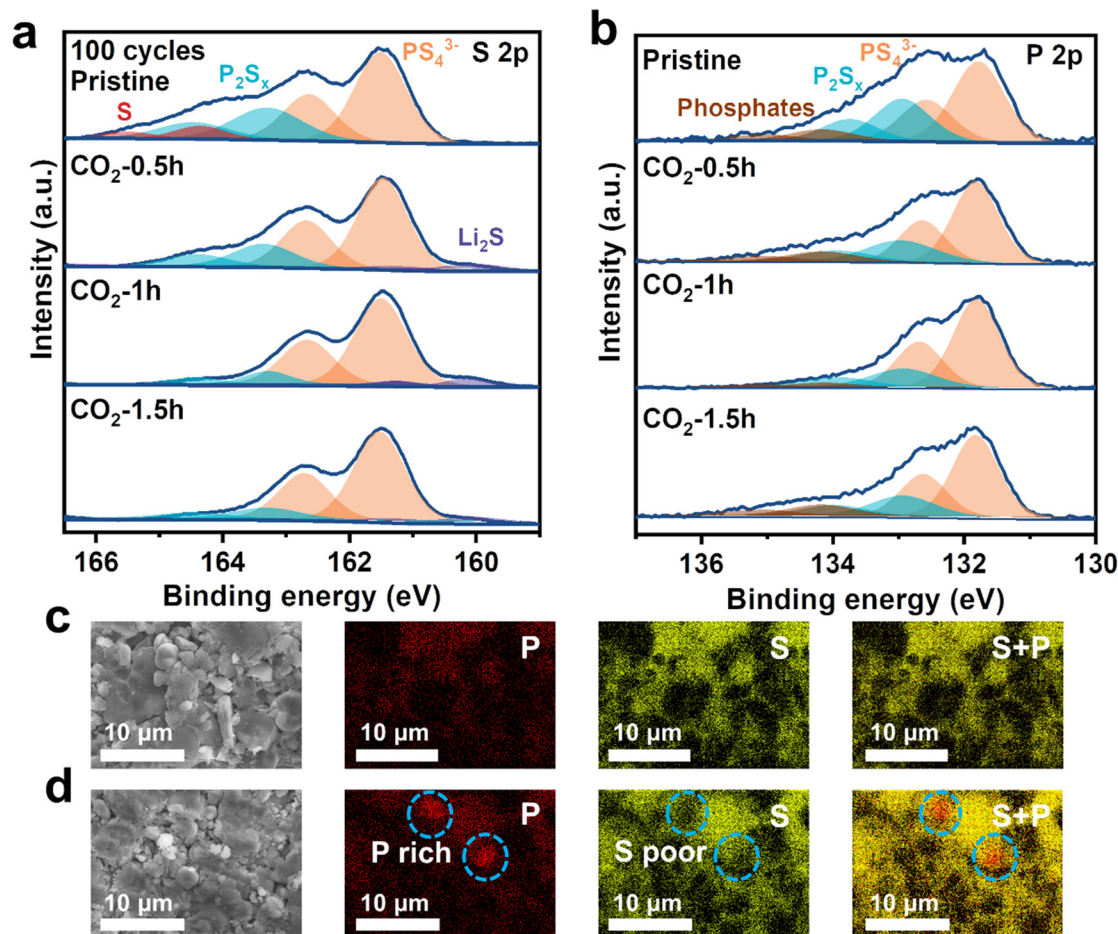


Fig. 3 Cathode electrolyte interface after 100 cycles. (a) XPS spectra of S 2p for the cathode. (b) XPS spectra of P 2p for the cathode. (c and d) EDS mapping of the CO₂-1h LPSC/LiCoO₂ composite (c) and the pristine LPSC/LiCoO₂ composite (d).

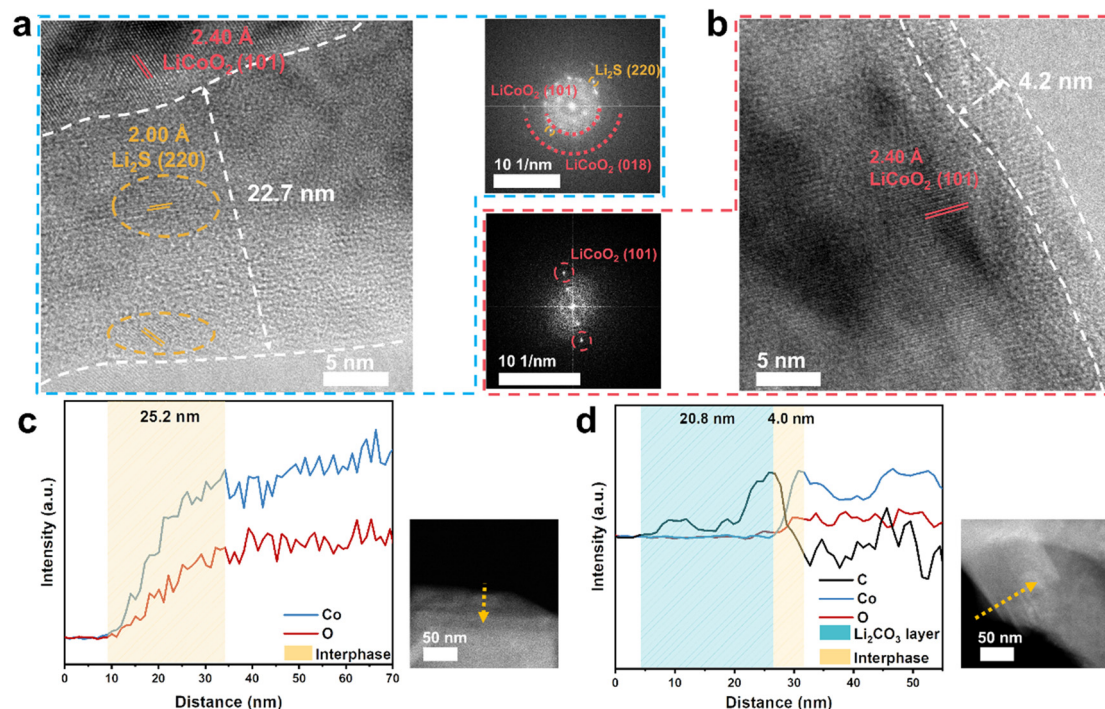


Fig. 4 Direct observation of CEI. (a and b) High-resolution TEM images and corresponding FFT for the LiCoO_2 with the pristine LPSC (a) and that with the CO_2 -1h LPSC (b) after 100 cycles. (c and d) EELS line profiles of Co/O/C for the LiCoO_2 with the pristine LPSC (c) and the LiCoO_2 with the CO_2 -1h LPSC (d) after 100 cycles.

2.4. Fabricating $\text{Li}_6\text{PS}_5\text{Cl}$ -based ASSBs in a dry room

The above results provide proof of concept that ASSBs with gas-treated LPSC show much-improved cycling stability and rate performance due to the reduced interfacial reaction and enhanced interfacial stability. When considering the feasibility and economic efficiency of this method for practical large-scale manufacturing, it is better to engineer the LPSC on-site during ASSB assembly in a dry room, which could avoid additional costly pretreatment processes (time, materials, and setups) and more importantly is compatible with current battery manufacture. Therefore, we demonstrate this concept in a small dry room (simulated in a glovebox, filled in synthetic air with adjustable CO_2 concentrations, dew point of $-25\text{ }^\circ\text{C}$ to $-30\text{ }^\circ\text{C}$). The ASSBs were assembled in this atmosphere using the pristine LPSC and it takes about 30 min, during which the pristine LPSC materials react with the mixed gases and form a surface protection layer (Fig. 1a) dominated by Li_2CO_3 without any Li_2O and Li_3N as evidenced by the XPS spectra (Fig. 5b and Fig. S25, ESI[†]). Consequently, the ASSBs fabricated in the dry room show superior performance of both reversible capacity and cycling stability over that assembled in the Ar-filled glovebox as did in most laboratories (Fig. 5a and Fig. S26, ESI[†]). A higher CO_2 concentration (45.8% vs. 0.075%) is better since more Li_2CO_3 is formed (Fig. 5b) and protects the LPSC, resulting in lower interfacial resistance (Fig. 5c). Note that the concentration of $\sim 0.075\%$ CO_2 is in the range of that in the actual dry room atmosphere. The enhanced performance implies an unexpected fact that the LPSC not only is compatible with current battery manufacture in the dry room but also

works better which will boost the practical fabrication and application of high-energy SSEs-based ASSBs.

The above results provide some new insights into the practicability of sulfide electrolytes regarding their biggest challenges to the air-stability and interfacial stability, especially with high-voltage cathode materials. These results demonstrate that the rate-determining step for the reaction kinetic of ASSBs lies more on the interfacial stability than the ionic conductivity of SSEs. Thus, constructing a stable low-resistance interface is essential for achieving high-performance ASSBs even at expense of the ionic conductivity of SSEs. In this sense, avoiding direct contact between SSEs and electrode materials by coating is an effective way to minimize their interfacial reaction. Currently, coating cathode particles with ionically conductive but electronically insulating materials, such as LiNbO_3 , is widely adopted to alleviate the interfacial instability of sulfide electrolytes whereas, the electronic-insulated nature of coating materials, like LiNbO_3 ($\sim 10^{-11}\text{ S cm}^{-1}$), will hinder the charge transfer between cathode particles. This is also true when Li_2CO_3 is coated on the surface of LiCoO_2 , which was obtained *via* annealing it at $600\text{ }^\circ\text{C}$ in the CO_2 atmosphere according to previous works.^{44,45} The existence of Li_2CO_3 was verified by XPS (Fig. S27a, ESI[†]) and TEM results showed a very thin ($\sim 3\text{ nm}$) continuous amorphous layer on the surface of LiCoO_2 (Fig. S27b, ESI[†]). The Li_2CO_3 -coated LiCoO_2 displays improved cycling performance compared to the uncoated one (Fig. S27c, ESI[†]), which indeed proves that Li_2CO_3 coating is helpful to hinder the interfacial reaction between the LiCoO_2 and LPSC. However, like LiNbO_3 coating, Li_2CO_3

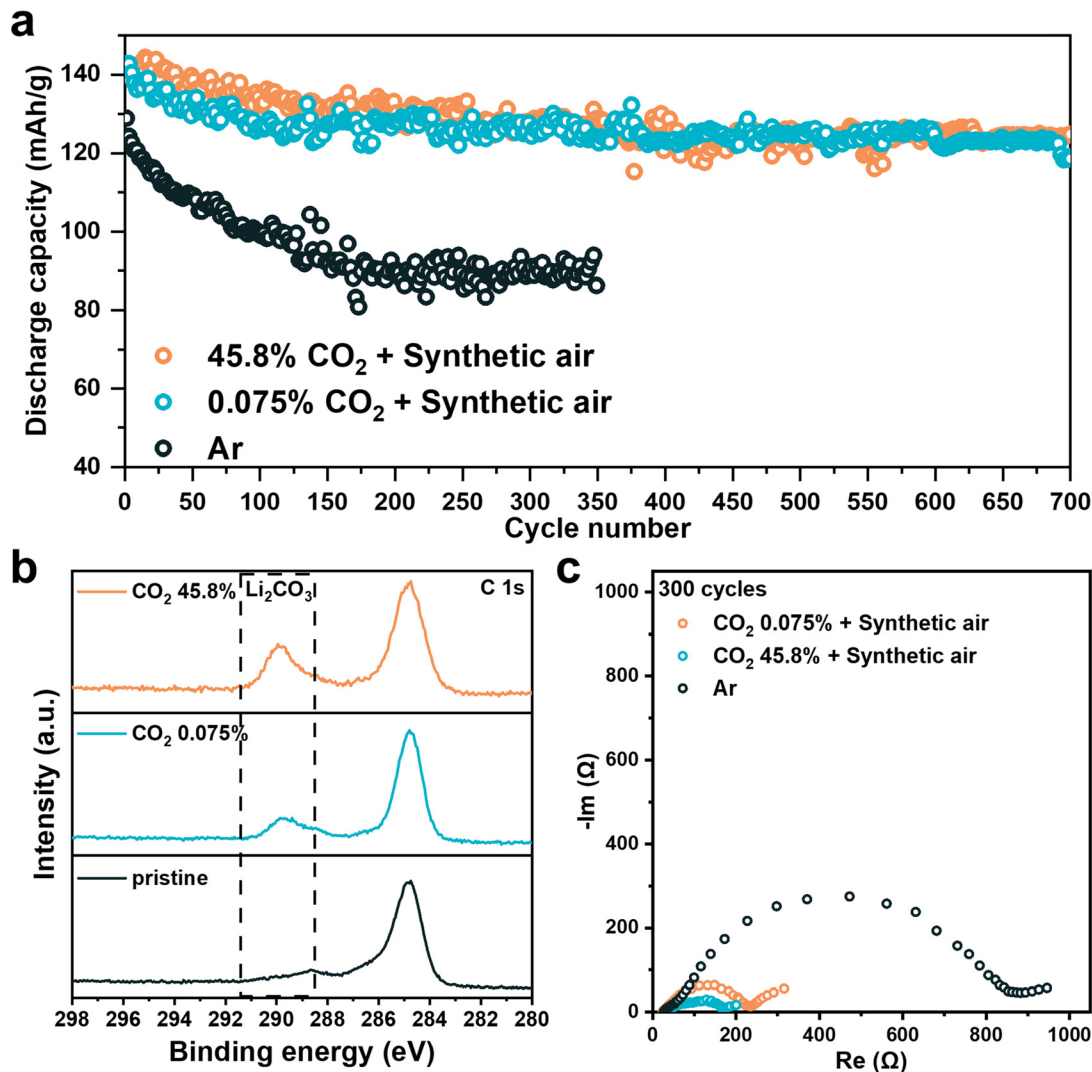


Fig. 5 Performance of ASSBs assembled in different atmospheres with the pristine LPSC electrolyte. (a) Cycling performance of the ASSBs assembled in different atmospheres with the pristine LPSC electrolyte and LiCoO₂ cathode at 0.5C rate. (b) The XPS C 1s spectra of the pristine LPSC materials after exposure to different atmospheres for 30 min. (c) Impedance spectra of ASSBs after 300 cycles.

coating on the surface of cathode particle shows worse cycling performance than that coating on the LPSC since the insulating coating layer consisting of Li₂CO₃ or LiNbO₃ will impede the electron transportation between cathode particles (Fig. S27d, ESI[†]). Instead, coating the SSE particles could avoid such issues and lead to superior cycling performance. Besides, coating LPSC with Li₂CO₃ further reduces the electronic conductivity of LPSC (from $1.53 \times 10^{-11} \text{ S cm}^{-1}$ to $2.1 \times 10^{-11} \text{ S cm}^{-1}$, Fig. S28, ESI[†]), which is believed helpful to hinder the growth of Li dendrites.^{20,46} The most important is that coating the SSEs also contributes to enhancing the air stability of sulfide electrolytes. This kind of treatment is compatible with the current battery fabrication in the dry room and does not require any additional modification. The enhanced performance of sulfide-based ASSBs fabricated in the dry room also demonstrates the feasibility and merits of sulfide electrolytes for practical use.

3. Conclusions

A simple gas–solid reaction was proposed to enhance the stability of sulfide electrolytes in the air and against the high-voltage oxides by surface coating. The spontaneous reactions between LPSC and CO₂ at room temperature form an amorphous Li₂CO₃ layer on the LPSC surface, which was confirmed by XPS, TOF-SIMS, and cryo-TEM. This protective layer not only enhances the toleration to the moisture but also dramatically improves the electrochemical performance of ASSBs coupled with bare LiCoO₂ cycled at a high voltage of up to 4.5 V vs. Li⁺/Li. In particular, the ASSB with LPSC pretreated in CO₂ for 1 h shows the best rate performance (65 mA h g⁻¹ at 3C) and excellent cycling retention (89.4% retention over 2100 cycles). This superior performance is ascribed to the reduced interfacial resistance enabled by Li₂CO₃ coating. Furthermore, we unravel the feasibility of fabricating the sulfide-based ASSBs in the dry room without additional costly pretreatment, showing

enhanced performance when compared with that assembled in a pure Ar atmosphere. These new insights will accelerate the scalable application of sulfide-based ASSBs.

Author contributions

X. Z., X. W., and Z. W. conceived the idea and designed the project. X. L. performed XPS measurements. S. W. and R. X. conducted DFT calculations. Q. L. performed Raman tests. X. Z. performed all the other data collection and analysis. S. W. conducted cryo-TEM tests. D. S., X. Y., H. L., M. C., Z. W., L. Z., Y. L., L. Z., Z. W., and L. C. contributed to discussions and interpretation of results. X. Z., X. W., and Z. W. co-wrote the manuscript, with input from all authors.

Conflicts of interest

The authors declare no competing interests.

Acknowledgements

The authors are thankful for the financial support from the Natural Science Foundation of Beijing (grant no. Z200013), and the National Key Research and Development Program of China (grant no. 2022YFB2502200).

References

- 1 Y. Liang, H. Liu, G. Wang, C. Wang, Y. Ni, C. W. Nan and L. Z. Fan, *InfoMat*, 2022, **4**, e12292.
- 2 K. B. Hatzell, X. C. Chen, C. L. Cobb, N. P. Dasgupta, M. B. Dixit, L. E. Marbella, M. T. McDowell, P. P. Mukherjee, A. Verma and V. Viswanathan, *ACS Energy Lett.*, 2020, **5**, 922–934.
- 3 Q. Zhang, D. Cao, Y. Ma, A. Natan, P. Aurora and H. Zhu, *Adv. Mater.*, 2019, **31**, e1901131.
- 4 S. Su, J. Ma, L. Zhao, K. Lin, Q. Li, S. Lv, F. Kang and Y. B. He, *Carbon Energy*, 2021, **3**, 866–894.
- 5 S. Chen, D. Xie, G. Liu, J. P. Mwiszerwa, Q. Zhang, Y. Zhao, X. Xu and X. Yao, *Energy Storage Mater.*, 2018, **14**, 58–74.
- 6 Y. Nikodimos, C.-J. Huang, B. W. Taklu, W.-N. Su and B. J. Hwang, *Energy Environ. Sci.*, 2022, **15**, 991–1033.
- 7 M. Lucero, S. Qiu and Z. Feng, *Carbon Energy*, 2021, **3**, 762–783.
- 8 H. Tsukasaki, H. Sano, K. Igarashi, A. Wakui, T. Yaguchi and S. Mori, *J. Power Sources*, 2022, **524**, 231085.
- 9 Y.-T. Chen, M. A. Marple, D. H. Tan, S.-Y. Ham, B. Sayahpour, W.-K. Li, H. Yang, J. B. Lee, H. J. Hah and E. A. Wu, *J. Mater. Chem. A*, 2022, **10**, 7155–7164.
- 10 P. Lu, L. Liu, S. Wang, J. Xu, J. Peng, W. Yan, Q. Wang, H. Li, L. Chen and F. Wu, *Adv. Mater.*, 2021, **33**, e2100921.
- 11 D. H. Tan, E. A. Wu, H. Nguyen, Z. Chen, M. A. Marple, J.-M. Dour, X. Wang, H. Yang, A. Banerjee and Y. S. Meng, *ACS Energy Lett.*, 2019, **4**, 2418–2427.
- 12 H. Wang, J. Zhu, Y. Su, Z. Gong and Y. Yang, *Sci. China: Chem.*, 2021, **64**, 879–898.
- 13 A. Banerjee, X. Wang, C. Fang, E. A. Wu and Y. S. Meng, *Chem. Rev.*, 2020, **120**, 6878–6933.
- 14 J. Zhang, C. Zheng, L. Li, Y. Xia, H. Huang, Y. Gan, C. Liang, X. He, X. Tao and W. Zhang, *Adv. Energy Mater.*, 2020, **10**, 1903311.
- 15 F. Walther, F. Strauss, X. Wu, B. Mogwitz, J. Hertle, J. Sann, M. Rohnke, T. Brezesinski and J. r Janek, *Chem. Mater.*, 2021, **33**, 2110–2125.
- 16 S. H. Jung, K. Oh, Y. J. Nam, D. Y. Oh, P. Brüner, K. Kang and Y. S. Jung, *Chem. Mater.*, 2018, **30**, 8190–8200.
- 17 L. Wang, R. Xie, B. Chen, X. Yu, J. Ma, C. Li, Z. Hu, X. Sun, C. Xu and S. Dong, *Nat. Commun.*, 2020, **11**, 1–9.
- 18 X. Li, L. Jin, D. Song, H. Zhang, X. Shi, Z. Wang, L. Zhang and L. Zhu, *J. Energy Chem.*, 2020, **40**, 39–45.
- 19 C. Wang, J. Liang, M. Jiang, X. Li, S. Mukherjee, K. Adair, M. Zheng, Y. Zhao, F. Zhao and S. Zhang, *Nano Energy*, 2020, **76**, 105015.
- 20 L. Zhou, T.-T. Zuo, C. Y. Kwok, S. Y. Kim, A. Assoud, Q. Zhang, J. Janek and L. F. Nazar, *Nat. Energy*, 2022, **7**, 83–93.
- 21 W. Huang, J. Wang, M. R. Braun, Z. Zhang, Y. Li, D. T. Boyle, P. C. McIntyre and Y. Cui, *Matter*, 2019, **1**, 1232–1245.
- 22 B. Han, Z. Zhang, Y. Zou, K. Xu, G. Xu, H. Wang, H. Meng, Y. Deng, J. Li and M. Gu, *Adv. Mater.*, 2021, **33**, 2100404.
- 23 K. Nishikawa and K. Shinoda, *J. Phys. Chem. Lett.*, 2021, **12**, 3922–3927.
- 24 A. Banerjee, H. Tang, X. Wang, J.-H. Cheng, H. Nguyen, M. Zhang, D. H. Tan, T. A. Wynn, E. A. Wu and J.-M. Dour, *ACS Appl. Mater. Inter.*, 2019, **11**, 43138–43145.
- 25 H. Xu, G. Cao, Y. Shen, Y. Yu, J. Hu, Z. Wang and G. Shao, *Energy Environ. Mater.*, 2022, **5**, 852–864.
- 26 Z. Zhang, L. Zhang, X. Yan, H. Wang, Y. Liu, C. Yu, X. Cao, L. van Eijck and B. Wen, *J. Power Sources*, 2019, **410**, 162–170.
- 27 B. Zhang, M. Weng, Z. Lin, Y. Feng, L. Yang, L. W. Wang and F. Pan, *Small*, 2020, **16**, 1906374.
- 28 R. Chen, Q. Li, X. Yu, L. Chen and H. Li, *Chem. Rev.*, 2020, **120**, 6820–6877.
- 29 Y. Li, Z. Wang, Y. Cao, F. Du, C. Chen, Z. Cui and X. Guo, *Electrochim. Acta*, 2015, **180**, 37–42.
- 30 W. Lu, M. Xue and C. Zhang, *Energy Storage Mater.*, 2021, **39**, 108–129.
- 31 G. Liu, W. Weng, Z. Zhang, L. Wu, J. Yang and X. Yao, *Nano Lett.*, 2020, **20**, 6660–6665.
- 32 S. H. Jung, K. Oh, Y. J. Nam, D. Y. Oh, P. Brüner, K. Kang and Y. S. Jung, *Chem. Mater.*, 2018, **30**, 8190–8200.
- 33 F. Strauss, J. H. Teo, J. Maibach, A.-Y. Kim, A. Mazilkin, J. R. Janek and T. Brezesinski, *ACS Appl. Mater. Interfaces*, 2020, **12**, 57146–57154.
- 34 J. Zhang, C. Zheng, L. Li, Y. Xia, H. Huang, Y. Gan, C. Liang, X. He, X. Tao and W. Zhang, *Adv. Energy Mater.*, 2020, **10**, 2070017.
- 35 J. Auvergniot, A. Cassel, J.-B. Ledeuil, V. Viallet, V. Seznec and R. Dedryvère, *Chem. Mater.*, 2017, **29**, 3883–3890.
- 36 Z. Sun, Y. Lai, N. Lv, Y. Hu, B. Li, S. Jing, L. Jiang, M. Jia, J. Li and S. Chen, *Adv. Mater. Interfaces*, 2021, **8**, 2100624.

- 37 L. Wang, X. Sun, J. Ma, B. Chen, C. Li, J. Li, L. Chang, X. Yu, T. S. Chan and Z. Hu, *Adv. Energy Mater.*, 2021, **11**, 2100881.
- 38 Y. Chen, W. Li, C. Sun, J. Jin, Q. Wang, X. Chen, W. Zha and Z. Wen, *Adv. Energy Mater.*, 2021, **11**, 2002545.
- 39 W. Zhang, T. Leichtweiß, S. P. Culver, R. Koerver, D. Das, D. A. Weber, W. G. Zeier and J. r Janek, *ACS Appl. Mater. Inter.*, 2017, **9**, 35888–35896.
- 40 H. Wan, J. Zhang, J. Xia, X. Ji, X. He, S. Liu and C. Wang, *Adv. Funct. Mater.*, 2022, **32**, 2110876.
- 41 W. Zhang, F. H. Richter, S. P. Culver, T. Leichtweiss, J. G. Lozano, C. Dietrich, P. G. Bruce, W. G. Zeier and J. r Janek, *ACS Appl. Mater. Interfaces*, 2018, **10**, 22226–22236.
- 42 A. Sakuda, A. Hayashi and M. Tatsumisago, *Chem. Mater.*, 2010, **22**, 949–956.
- 43 Y. Wu, K. Zhou, F. Ren, Y. Ha, Z. Liang, X. Zheng, Z. Wang, W. Yang, M. Zhang and M. Luo, *Energy Environ. Sci.*, 2022, **15**, 3470–3482.
- 44 H. Sheng, X. H. Meng, D. D. Xiao, M. Fan, W. P. Chen, J. Wan, J. Tang, Y. G. Zou, F. Wang and R. Wen, *Adv. Mater.*, 2022, **34**, 2108947.
- 45 Q. Tang, X. Dai, Z. Wang, F. Wu, Y. Mai, Y. Gu and Y. Deng, *Ceram. Int.*, 2021, **47**, 19374–19383.
- 46 F. Han, A. S. Westover, J. Yue, X. Fan, F. Wang, M. Chi, D. N. Leonard, N. J. Dudney, H. Wang and C. Wang, *Nat. Energy*, 2019, **4**, 187–196.